


## Article

# Energy-Efficiency-Oriented Spatial Configuration of VRV Outdoor Units in an Equipment Layer Under Background Wind Conditions

Lin Liu, Haoran Huang and Xiaoyu Tian \* 

School of Civil and Transportation Engineering, Guangdong University of Technology, Guangzhou 510006, China; liulin@gdut.edu.cn (L.L.); 2112109130@mail2.gdut.edu.cn (H.H.)

\* Correspondence: tianxiaoyujian@163.com

**Abstract:** This study provides a spatial configuration method to improve the cooling efficiency of multiple VRV outdoor units placed on equipment layers with high floors. Relevant factors include wind parameters, the placement of multiple outdoor units, and louver. A total of 96 cases were designed. CFD simulations were used to obtain the inlet air temperature distributions of multiple outdoor units and then calculate their cooling efficiency. The results found that these factors have effects on the average cooling efficiency of outdoor units in a single row to a certain extent. The influencing degrees of these factors, from large to small, were the louver angle, wind parameters, and the placement of multiple outdoor units. When the cooling efficiency of outdoor units was maximum and the louver angle was 15°, the louvers could be oriented perpendicular to the dominant wind direction (90°) when wind speed was  $\geq 6$  m/s, and the unit spacing was 600 mm. Based on this, when the number of outdoor units was expanded in the limited space, staggered arrangements with different directions of heat exchange surfaces were a recommended optimization layout. This study provides technical support for improving the working efficiency of VRV outdoor units in an equipment layer.

**Keywords:** VRV; equipment layer; cooling efficiency; inlet air temperature; influencing factors



**Citation:** Liu, L.; Huang, H.; Tian, X. Energy-Efficiency-Oriented Spatial Configuration of VRV Outdoor Units in an Equipment Layer Under Background Wind Conditions. *Buildings* **2024**, *14*, 3681. <https://doi.org/10.3390/buildings14113681>

Academic Editor: Constantinos A. Balaras

Received: 12 October 2024

Revised: 15 November 2024

Accepted: 16 November 2024

Published: 19 November 2024



**Copyright:** © 2024 by the authors. Licensee MDPI, Basel, Switzerland. This article is an open access article distributed under the terms and conditions of the Creative Commons Attribution (CC BY) license (<https://creativecommons.org/licenses/by/4.0/>).

## 1. Introduction

Rapid urbanization, expanding population, and increased air temperature have elevated energy demand [1,2]. In 2019, the International Energy Agency reported that global electricity consumption reached 25,027.3 TWh and showed an increasing trend [3]. Global carbon dioxide emissions increased from 22.28 Gt in 1990 to 35.47 Gt in 2019 [4]. Building operations generate about 10 billion tons of CO<sub>2</sub> emissions, accounting for about 37% of global emissions [5]. However, the energy consumption of air conditioning systems contributed more than 40%, especially for commercial buildings. For example, air conditioning systems accounted for 47.17% of the total energy consumption of office buildings in Guangzhou, China [6], and 50% of the total energy consumption of high-rise public buildings in Chongqing, China [7]. Therefore, how to control air conditioning energy consumption is a crucial factor in reducing anthropogenic carbon emissions.

Variable Refrigerant Volume (VRV) has been widely used to meet public buildings' cooling/heating demands due to its saving space, easy installation, reliable operation, and flexibility [8,9]. A primary factor influencing the higher energy consumption was the heat exchange effects of VRV outdoor units, which then influenced the operating efficiency of outdoor units. The outdoor unit is like an air-cooled heat exchanger; its heat exchange effects depend on external airflow. Especially, urbanization has resulted in the transformation of natural underlying surfaces into high-rise and dense building clusters [10,11]. Usually, the outdoor units are placed on the roofs or on the top floor of the building. However, some outdoor units are inevitably placed on the middle floors of the

building. Due to wind speed, wind pressure, louvers, and other factors, indoor airflow could be affected, and then outdoor units' cooling efficiency can be worsened. In severe cases, it may cause the units to shut down. For example, Kabeel et al. found that the supply air temperature was reduced by 21% and the coefficient of performance improved by 71% in a hybrid air conditioning system using an indirect evaporation cooler with an internal baffle as pre-cooling units compared to previous designs of the hybrid air conditioning system [12]. Yau and Pean found that the total cooling capacity of the system is decreased by 2% when the outdoor temperature is increased by 1 °C [13]. Therefore, it is necessary to explore an optimization design method to improve the cooling performance of outdoor units in an equipment layer. Before that, it is first necessary to determine which factors influence the inlet air temperature of outdoor units.

Nowadays, many studies have investigated the factors influencing the inlet air temperature of air conditioning systems' outdoor units [14–17]. These factors mainly include the louver [18–21], placement of air conditioner units [22–26], layout of the outdoor unit [14,23,27,28], horizontal distance between the condenser unit and wall [29–35], unit spacing [35–37], building re-entrant shapes [38], outdoor wind speed [39–41], and directions of exhaust [42]. These studies provided some recommended parameters to obtain a lower inlet air temperature, namely a higher cooling efficiency. For example, in these studies, they observed that the inlet air temperature of outdoor units increases with the increase in louver angle and the recommended louver angle was not higher than 15°. Chow et al. found that a face-to-face layout of outdoor units can be appropriate [14]. Some studies observed that the staggered placement of the front and rear outdoor units effectively reduces the inlet air temperature of the outdoor units [25,42]. A detailed literature review is shown in Table 1. However, three limitations existed in the literature. Firstly, most of these studies only explored the effect of a single factor or some factors without considering the comprehensive impact of these factors, and the influencing degree of these factors was not explored. Secondly, these studies investigated the inlet air temperature of outdoor units placed outside buildings, not considering the scenario of outdoor units inside buildings and placed on high floors of the building. Thirdly, the comprehensive effect between background wind parameters was not explored in these studies.

**Table 1.** A detailed literature review on the outdoor units of air conditioners.

Reference	Influencing Factors	Results
Chow et al., 2002 [14] Locations: Hongkong, China	condenser unit layouts	<ul style="list-style-type: none"> <li>The effect of 10 types of condensing unit layouts in the building re-entrant on the COP of air conditioning systems. The results found that face-to-face layouts of AC units can be an appropriate layout.</li> </ul>
Chow et al., 2002 [15] Locations: Hongkong, China	louver, terrace	<ul style="list-style-type: none"> <li>The effect of outdoor units in building re-entrant on the condenser units' surrounding temperature and the energy coefficient of the AC units. The results obtained an optimal arrangement.</li> </ul>
Chen et al., 2009 [18] Location: Fushan, China	louver	<ul style="list-style-type: none"> <li>Operating environments can be improved when the louver angle decreases.</li> </ul>
Yang, 2017 [19] Locations: Shandong, China	louver	<ul style="list-style-type: none"> <li>The inlet air temperature increases as the inclination angle of the louvers increases.</li> </ul>
Liu et al., 2017 [20] Location: Qingdao, China	louver	<ul style="list-style-type: none"> <li>Operating environments can be improved when the louver angle decreases. The louver angle was recommended as 15° or less than 15°.</li> </ul>

Table 1. Cont.

Reference	Influencing Factors	Results
Yang et al. [21] Locations: Chongqing, China	louver	<ul style="list-style-type: none"> <li>The recommended parameters when the operating environment was best were that the louver spacing is 80 mm and its angle is 10°.</li> </ul>
Chow et al., 2001 [22] Locations: Hongkong, China	placement of air conditioner units	<ul style="list-style-type: none"> <li>The effect of airflow characteristics around the condenser units on the AC characteristics. The results show that discharging the outdoor units' air into a light well leads to better unit performance and low power consumption compared to the case of installing the outdoor units in a building re-entrant.</li> </ul>
Nada and Said, 2017 [23] Location: Benha, Egypt	different arrangements	<ul style="list-style-type: none"> <li>In the case of an open-bottom shaft, it is preferable to distribute all the outdoor units on one wall of the shaft, except that at the top two levels it is preferable that the units be distributed on two adjacent walls in staggered arrangements.</li> </ul>
Li 2018 [24] Locations: Harbin, China	placement, louver	<ul style="list-style-type: none"> <li>Investigate the relationship between the inlet air temperature of outdoor units and factors including distance between the units and the wall, distance from the louver, louver angle, louver spacing, outdoor wind speed, and outdoor air temperature.</li> </ul>
Zhou et al., 2010 [25] Locations: Beijing, China	placement	<ul style="list-style-type: none"> <li>The incoming wind speed significantly affects the heat dissipation of outdoor units.</li> </ul>
Zhao et al., 2017 [26] Locations: Guangzhou, China	placement of outdoor units	<ul style="list-style-type: none"> <li>The important factors influencing the thermal environment of the outdoor units are the distance between the units and the wall.</li> </ul>
Yu et al., 2022 [27] Locations: Shandong, China	layout of outdoor unit and placement	<ul style="list-style-type: none"> <li>The CFD simulation results found that the outdoor units' performance is optimal when one outdoor unit is installed close to the louver and the other is lifted away from the louvers at the top of the groove.</li> </ul>
Huang et al., 2017 [28] Locations: Beijing, China	layout of outdoor units	<ul style="list-style-type: none"> <li>The staggered placement of the front and rear outdoor units effectively reduces the inlet air temperature of the outdoor units.</li> </ul>
Avara and Daneshgar, 2008 [29] Location: Bushehr, Iran	spacing between two sidewalls, distance	<ul style="list-style-type: none"> <li>The effect of the spacing between the two supporting walls of the outdoor units on the on-coil temperature of condenser units.</li> <li>Recommended various optimum distances between the outdoor AC unit and supporting wall in different spacing between the sidewalls.</li> </ul>
Xue et al., 2007 [30] Location: Henan, China Climate: Temperate	horizontal distance between condenser unit and wall, the space per condensing unit	<ul style="list-style-type: none"> <li>Exploring the air temperature and wind velocity distribution around the outdoor units.</li> <li>A distance between two sidewalls of 7 m is needed to keep the temperature raised less than 10 °C.</li> <li>The space per condensing unit should be at least larger than 18.2 m<sup>2</sup>.</li> </ul>

Table 1. Cont.

Reference	Influencing Factors	Results
Duan et al., 2016 [31] Location: Beijing, China	distance between neighbouring outdoor units, louver spacing, louver angle, and arrangement style	<ul style="list-style-type: none"> <li>To reduce operation temperature and save energy, the following design points are recommended: Vertical arrangement for outdoor units. A larger distance between neighboring outdoor units. Smaller louver for the louver angle. 100 degrees for the louver angle.</li> </ul>
Harithkhan et al., 2021 [32] Locations: Moratuwa, Sri Lanka	horizontal distance between condenser unit and wall	<ul style="list-style-type: none"> <li>The selected building with a re-entrant size of 6 m × 2.5 m distance of 1.5 m from the exterior wall was found to be the optimum position for the condenser.</li> </ul>
Jiang 2013 [33] Locations: Tianjin, China	distance between the units and wall, louver	<ul style="list-style-type: none"> <li>It is recommended that the distance between the outdoor unit condenser and the wall be greater than 100 mm, the distance between the left side of the outdoor unit and the wall be at least 200 mm, the distance between the fan and the louver be around 100 mm, the louver angle do not exceed 20°, and the direction be downward with a minimum louver spacing of 50 mm.</li> </ul>
Bruelisauer et al., 2013 [34] Location: National University of Singapore Singapore	spacing between two sidewalls, horizontal distance between condenser unit and wall	<ul style="list-style-type: none"> <li>The air temperature in the recessed space increased continuously to reach up to 12.7 °C higher temperatures than undisturbed conditions at the top of 20 floors when air conditioners were switched on.</li> <li>The inlet temperature increases by 9.0 °C on the lowest level along with the 50 °C maximum inlet temperature and 59 °C outlet temperature.</li> </ul>
Zhang, 2009 [35] Locations: Dalian, China	Unit spacing, the distance between the units and pillars	<ul style="list-style-type: none"> <li>The maximum distance between outdoor units is 0.2 m, the maximum distance from the pillar is 0.8 m, and the maximum distance between multiple outdoor unit arrays is 0.8 m</li> </ul>
Zhang et al., 2008 [36] Locations: -	Unit spacing	<ul style="list-style-type: none"> <li>Outdoor units of VRV have lower inlet air temperature when the unit spacing is greater than 1.65 m.</li> </ul>
Wei and Jiang, 2021 [37] Locations: Zhejiang, China	Unit spacing	<ul style="list-style-type: none"> <li>The inlet air temperature is close to the background air temperature when unit spacing is greater than 2 m</li> </ul>
Chow et al., 2000 [38] Locations: Hongkong, China	building re-entrant shapes	<ul style="list-style-type: none"> <li>Explored the effect of different re-entrant shapes (T-, I- and L-shapes) on which the outdoor AC units were placed. The results found that the T-shaped re-entrant showed lower outdoor air temperatures around the buildings compared with the I- and L-shaped re-entrants.</li> </ul>
Choi et al., 2005 [39] Location: Seoul, South Korea	Wind speed, wind direction and layout of the outdoor unit	<ul style="list-style-type: none"> <li>The performance of the condensers above the 30th floor decreased.</li> <li>The performance of heat dissipation of the condensers for the higher floor drooped significantly when the frontal- and side-winds were greater than 4 m/s and 8 m/s, respectively.</li> </ul>
Li and Liu, 2019 [40] Locations: Shandong, China	Wind speed	<ul style="list-style-type: none"> <li>To effectively solve the airflow short circuit, the inlet and exhaust surfaces of the unit are not in the same direction. The airflow velocity of the incoming air should be controlled below 1–1.5 m/s.</li> </ul>

Table 1. Cont.

Reference	Influencing Factors	Results
Zi and Wu, 2017 [41] Locations: Guangdong, China	Wind speed	<ul style="list-style-type: none"> <li>Keeping the exhaust direction of the outdoor unit consistent.</li> </ul>
Ge et al., 2007 [42] Locations: Sichuan, China	Directions of exhaust	<ul style="list-style-type: none"> <li>Compared with the units with the same side of exhaust air, the units with the opposite side of exhaust air show better performance.</li> </ul>

Considering the above limitations, this study investigates an optimization method for the cooling efficiency of outdoor units in the equipment layer placed on the high floors of the buildings. Firstly, the factors influencing outdoor units' cooling efficiency were analyzed. These factors can be divided into three aspects: wind parameters, the placement of multiple outdoor units, and louvers. Wind parameters include wind speed and wind direction. The placement of multiple outdoor units includes unit spacing, the distance between the units and the front wall, and the distance between the unit and the left/right pillar. Secondly, an arrangement-combination method was used to design 96 cases. CFD simulations were used to obtain the overall inlet air temperature of these cases. The optimal parameter configuration of multiple outdoor units in a single row was obtained considering the maximum cooling efficiency. Finally, on this basis, an optimal layout for multiple outdoor units with an expanded dual row was obtained. This study provides a parametric and systematic optimization design method for obtaining a better cooling efficiency from multiple outdoor units placed on an equipment layer with high floors. It also contributes to the sustainable development of future society [43] and the analysis of energy efficiency factors in buildings in smart cities [44].

## 2. Methods

### 2.1. Cooling Efficiency Indicator

Figure 1a shows the circulation process and main hardware components of refrigerant in the VRV air conditioning system. In general, VRV systems mainly include indoor units and outdoor units. The outdoor units mainly involve two components: the condenser and compressor, which are used to deliver the outdoor air temperature to the indoors through air conditioning technology. The heat exchange between the refrigerant and the air occurs in the evaporator (indoors) and the condenser (outdoors). Ideally, the maximum cooling efficiency of the refrigeration machine ( $\varepsilon$ ) can be expressed as following formulas according to the vapor compression refrigeration cycle (a T-S diagram of the Carnot cycle was shown in Figure 1b when operating at the specific temperature  $T_k$  and  $T_0$  [45]).

$$\varepsilon = \frac{1}{T_k/T_0 - 1} \quad (1)$$

where  $T_0$  is the cooled temperature and  $T_k$  is the temperature of the heat source, namely the inlet air temperature.

It is assumed that  $T_z$  is the overall inlet air temperature of outdoor units, which can be expressed by each outdoor unit's inlet air temperature and its corresponding cooling capacity ratio ( $Q_i$ ) to the total cooling capacity ( $Q_z$ ). Its expression was

$$T_z = \sum_{k=1}^n (T_k \frac{Q_k}{Q_z}) \quad (2)$$

Based on formulas (1) and (2), the average cooling efficiency of refrigeration machines ( $\bar{\varepsilon}$ ) can be written as

$$\bar{\varepsilon} = \frac{1}{\sum_{k=1}^n (T_k \frac{Q_k}{Q_z}) / T_0 - 1} \quad (3)$$

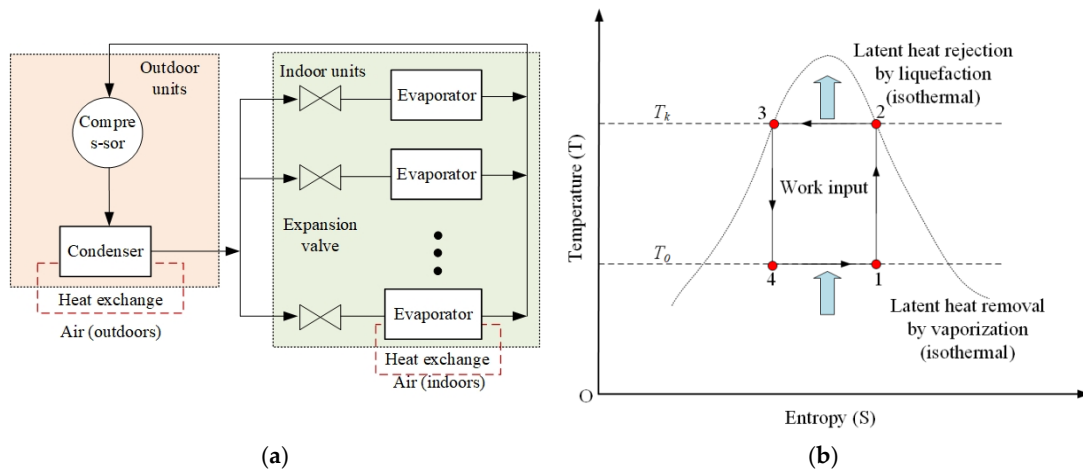


**Figure 1.** Principle of VRV air conditioning systems. (a) Schematic of VRV, (b) Carnot cycle.

## 2.2. Influencing Factors

In this study, the research object is the outdoor units of VRV, which are placed on the equipment layer of high-rise commercial buildings in Guangzhou, China. The equipment layer is located on the 44th floor of the building, which has a height of 4.5 m (see Figure 2) and is higher than 100 m from the ground. During a typical summer in Guangzhou, China, the average wind speed around the building is 1.9 m/s in 10 m of building height, the outdoor temperature is 35 °C, and southeast winds prevail. These air conditioning systems were used to provide the cooling/heating demands on the 43rd and 45th floors. Then, according to the cooling/heating demand, four outdoor units of VRV were arranged in parallel (see Figure 2a). Based on the results of the field investigation, a widely used VRV air conditioning system was selected. The specifications of the outdoor unit are presented in Table 2. The dimension of outdoor units is 1657 × 1240 × 765 mm<sup>3</sup> (L × W × H). The cooling capacity is 61.5 KW, and power consumption is 18.6 KW. The maximum inlet air temperature is 50 °C.

**Table 2.** The specifications of the outdoor unit.

Model	RUXYQ22AB
Cooling capacity (KW)	61.5
Power consumption (KW)	18.6
Dimension of outdoor unit (L × W × H, mm × mm × mm)	1657 × 1240 × 765
Air volume (m <sup>3</sup> /min)	271
Maximum inlet air temperature (°C)	50

According to the results of previous studies (see Table 1), the factors influencing the cooling efficiency of all outdoor units from the perspective of airflow could involve three categories. One is the louver angles. The louvers are always used for ventilation, air exchange, and rainproofing. The second one is the placement of multiple outdoor units in the equipment layer, including unit spacing (D1), distance between the units and the front wall (D2), and distance between the unit and the left/right pillars (D3), as shown in Figure 2b,c.

Besides that, background wind conditions include wind speed and direction. The prevailing wind direction in a season is basically unchanged. When the buildings are built, the windward and leeward sides of the building are already determined (see Figure 2d). The angle is the angle between the background wind direction and the louvers. However, the placement of the outdoor unit on which side of the building can be designed and planned.

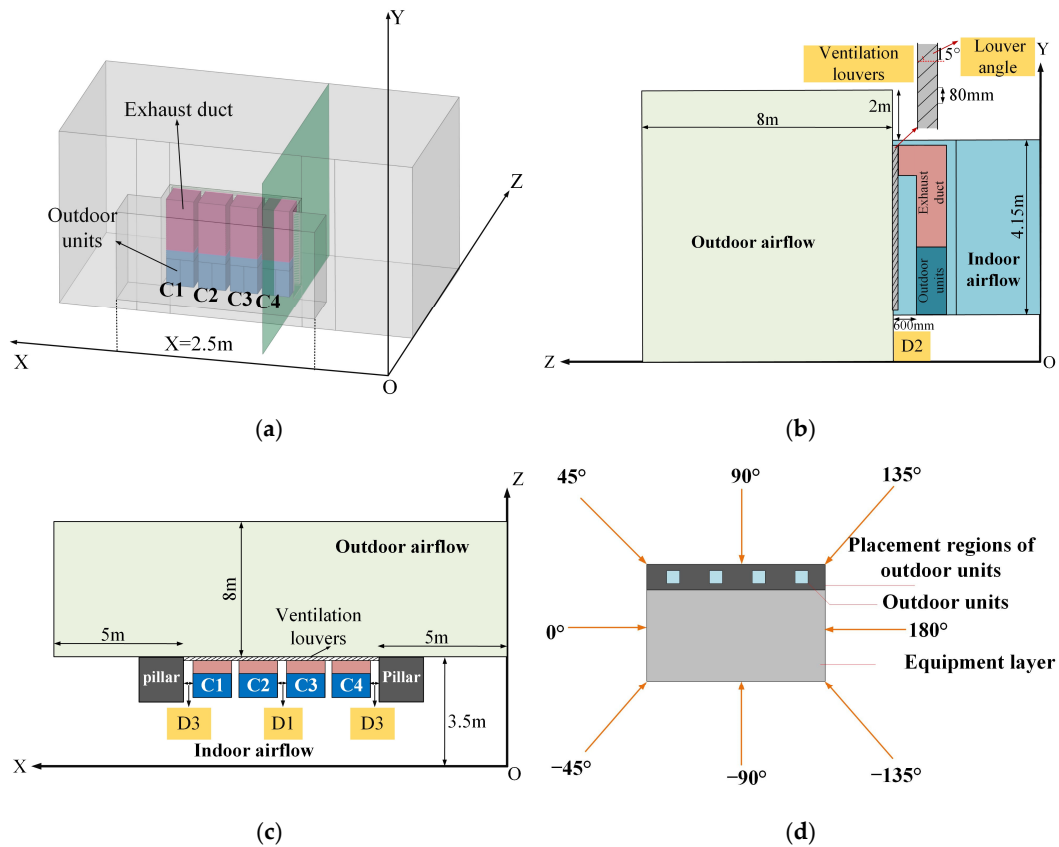


**Figure 2.** Schematic diagram of a numerical physical model. (a) 3D diagram, (b) side view, (c) vertical view, (d) wind directions.

### 2.3. Case Designs

Based on the results of previous studies and field investigations, a total of 96 cases were designed, including four angles of louver ( $45^\circ$ ,  $30^\circ$ ,  $15^\circ$ ,  $0^\circ$ ), three unit spacings (200, 400, and 600 mm), three distances between the unit and the left/right columns (200, 400, and 600 mm), three distances between the units and the front wall (400, 600, and 800 mm), three wind speeds (4, 6, and 8 m/s), and eight wind directions ( $-135^\circ$ ,  $-90^\circ$ ,  $-45^\circ$ ,  $0^\circ$ ,  $45^\circ$ ,  $90^\circ$ ,  $135^\circ$ ,  $180^\circ$ ). Table 3 lists the detailed parameter configurations for the main 12 basic cases. Among them, wind speeds were set as 6 m/s in Cases 1~10 and 4 and 8 m/s in Case 11 and Case 12, respectively. Each case involves eight wind directions.

**Table 3.** The parameter configurations of cases.

Cases	Louver Angle ( $^\circ$ )	D1 (mm)	D2 (mm)	D3 (mm)
1	45	200	600	200
2	30	200	600	200
3	15	200	600	200
4	0	200	600	200
5	15	400	600	200
6	15	600	600	200
7	15	200	400	200
8	15	200	800	200
9	15	200	600	400
10	15	200	600	600
11	15	200	600	200
12	15	200	600	200

## 2.4. CFD Simulations

### 2.4.1. Computational Domains

Computational domain was generated by using the SCDM 2024 software built in ANSYS, which was developed by SpaceClaim Corporation [46]. Its dimension was determined and calibrated based on the results of field investigations, including the dimensions of building layers, the number of external air conditioning units, the unit spacing, the distance between the units and the front wall, the distance between the unit and the left/right pillars, and the louver spacing. The domain mainly includes three parts: the building interior, the outdoor space, and the external air conditioning unit (see Figure 2a). The relevant information of the computational domains is shown in Figure 3a,b. In this study, to further reduce the computational cost, the computational domain was simplified through three assumptions:

- In the physical model, all walls were set as insulated walls, such as building exterior walls, louvers, exhaust systems, etc.
- Ignoring the effects of outdoor solar radiation, outdoor temperature was considered and set as 33.2 °C. The indoor temperature was set at 26 °C.
- All outdoor units were set to working at full loads and were regarded as a black-box-like heat source by ignoring their internal structure. The heat dissipation was the sum of the cooling capacity and cooling power consumption of the VRV system. The heat source per unit volume was 37,147 W/m<sup>3</sup>.

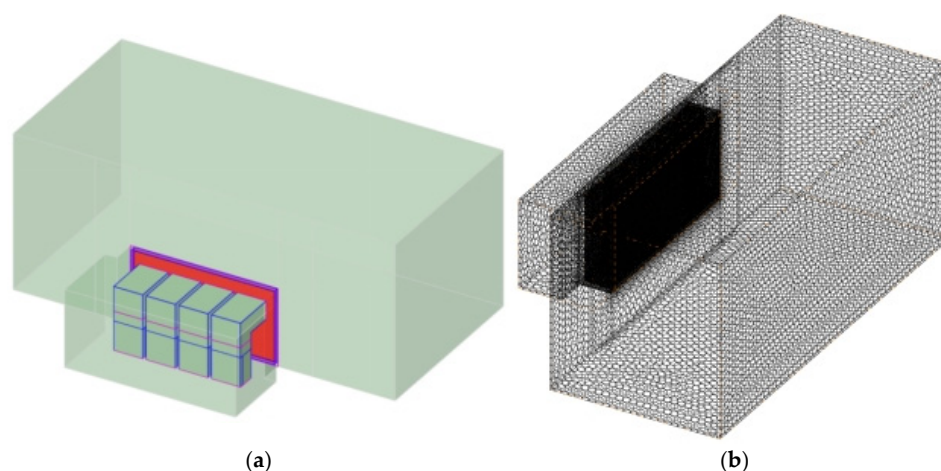


**Figure 3.** Computational domains and grids. (a) computational domains, (b) grid cells.

The computational grids were structured and created using a mosaic grid-generation technique to limit the total number of computational cells in the domain and improve the quality of grid topology [47]. The ANSYS Fluent Meshing [48] was used for the generation of computational grids (Figure 3b). All surface grids were spatially discretized with polyhedral cells, and the poly-hexforce cells were used in the external AC unit and automatically combined with the boundary layer grid near the surface walls. The Tecplot 360 software was used to visualize and analyze the results of the CFD simulation [49]. Table 4 lists the physical properties of the air. The specific heat capacity is 1.005 J/(kg·°C). Thermal conductivity is set as  $2.715 \times 10^{-2}$  W/m·K. The coefficient of thermal expansion is 0.0034.

**Table 4.** Physical properties of the air.

Parameters	Values
Density (kg/m <sup>3</sup> )	1.1465
Specific heat capacity (J/(kg·°C))	1.005
Thermal conductivity (W/m·K)	$2.715 \times 10^{-2}$
Viscosity (m·Pa·s)	$18.85 \times 10^{-4}$
Coefficient of thermal expansion	0.0034



### 2.4.2. Boundary Conditions

In this study, the main boundaries include the exterior walls of the equipment layer, casings of outdoor units, air ducts, louvers, fans of outdoor units, the air inlets of outdoor units, and the air inlets and outlets of the external computational domain. In this study, referring to existing relevant literature [15–42], the boundary conditions in ANSYS Fluent software 2024 r1 are set as shown in Table 5. As shown in Table 5, the main boundary conditions include the exterior wall, casing of outdoor units, air ducts, louvers, air inlets of outdoor units, fans of outdoor units, and corresponding computational domain.

**Table 5.** Boundary condition settings in ANSYS Fluent software 2024 r1.

Parts.	Types	Settings
Exterior walls	Adiabatic wall	
Casings of outdoor units	Adiabatic wall	Heat flux and heat radiation are 0
Air ducts	Adiabatic wall	
Louvers	Wall without thickness	0
Air inlets of outdoor units	Porous jump	$\alpha = 2.13e^{-6}$ , $C2 = 0.1997$ [47]
Fans of outdoor units	Fan	Pressure difference is set to the pressure at the rated air volume of outdoor units
Air inlets of the external computational domain	Velocity Inlet	$V = V_c \left(\frac{h}{h_c}\right)^n$ [48]
Outlets of external computational domain	Static pressure outlet	0 Pa

Note:  $V$  is the wind speed at a height.  $V_c$  is the wind speed of reference height, which is 1.9 m/s.  $h$  is a height.  $h_c$  is the reference height, which is 10 m.  $n$  is the roughness index, which is set as 0.4.

### 2.4.3. Solver Settings

The simulations were performed with the commercial ANSYS Fluent 2024r1 [50]. The RANS equation was solved in combination with the Standard k- $\epsilon$  model [29]. Finite volume discretization technology was used to solve the coupled partial differential equation and initial conditions in numerical modes. The SIMPLE algorithm was used for pressure–velocity coupling. Pressure interpolation was a second-order discretization scheme which was used for the pressure terms and the viscous terms of the governing equations. The pressure and momentum relaxation factors were set as 0.3 and 0.7, respectively. The volume and viscosity relaxation factors were 0.6 and 0.7, respectively. The momentum and turbulent energy relaxation factors were 0.6 and 0.9, respectively. Convergence was assumed to be obtained when reaching a minimum of  $10^{-6}$  for momentum.

The governing equations for airflow and heat transfer include the Mass conservation equation, the Momentum conservation equation and the Energy conservation equation. Their expressions are as follows:

- (a) Mass conservation equation:

$$\frac{\partial \rho}{\partial t} + \nabla \cdot \rho \vec{v} = 0 \quad (4)$$

where  $\rho$  is the pressure, Pa and  $\vec{v}$  is the velocity vector, m/s.

- (b) Momentum conservation equation:

$$\begin{aligned} \frac{\partial}{\partial t}(\rho \vec{v}) + \nabla \cdot (\rho \vec{v} \vec{v}) &= -\nabla \rho + \nabla \cdot (\bar{\tau}) + \rho \vec{g} + \vec{F} \\ \bar{\tau} &= \mu [(\nabla \vec{v} + \nabla(\vec{v})^T) - \frac{2}{3} \nabla \vec{v} I] \end{aligned} \quad (5)$$

where,  $\rho$  is the pressure, Pa,  $\vec{v}$  is the velocity vector,  $\vec{F}$  is the forces acting on micro-elements, and  $\bar{\tau}$  is the viscous stress.

(c) Energy conservation equation:

$$\frac{\partial(\rho T)}{\partial t} + \text{div}(\rho u T) = \text{div}\left(\frac{k}{c_p} \text{grad} T\right) + S_T \quad (6)$$

$$h = \int_{T_{ref}}^T c_p dT \text{ and } k_t = \frac{c_p \mu_t}{Pr_t}$$

where,  $T$  is the air temperature,  $k$  is the heat transfer coefficient,  $W/(m \cdot K)$ ,  $C_p$  is the specific heat capacity,  $J/(kg \cdot K)$ , and  $S_T$  is a viscous dissipation term.

### 2.5. Grid Independence Test

The grid independence was used to obtain the optimal number of computational grid cells based on a certain threshold. It indicates that the number of grid cells did not impact the simulation results when the threshold was reached. That is, when  $T_Z(m+1) - T_Z(m) < 0.01$  °C. Where  $m$  is the number of grid cells.

Independence tests were performed for five grid resolutions in total, and the numbers of grid cells were  $4.57707 \times 10^5$ ,  $8.57362 \times 10^5$ ,  $12.73952 \times 10^5$ ,  $14.05279 \times 10^5$ , and  $16.99537 \times 10^5$ . The results showed that the overall inlet air temperatures were 40.510, 39.490, 38.753, 38.752, and 38.753 °C, respectively. When the number of grids is not less than 1,273,952, the computational load and speed of computer hardware, and the prediction accuracy of the physical model, the grid size of  $12.73952 \times 10^5$  is selected for calculations in this study.

The detailed flowchart of this study is shown in Figure 4.

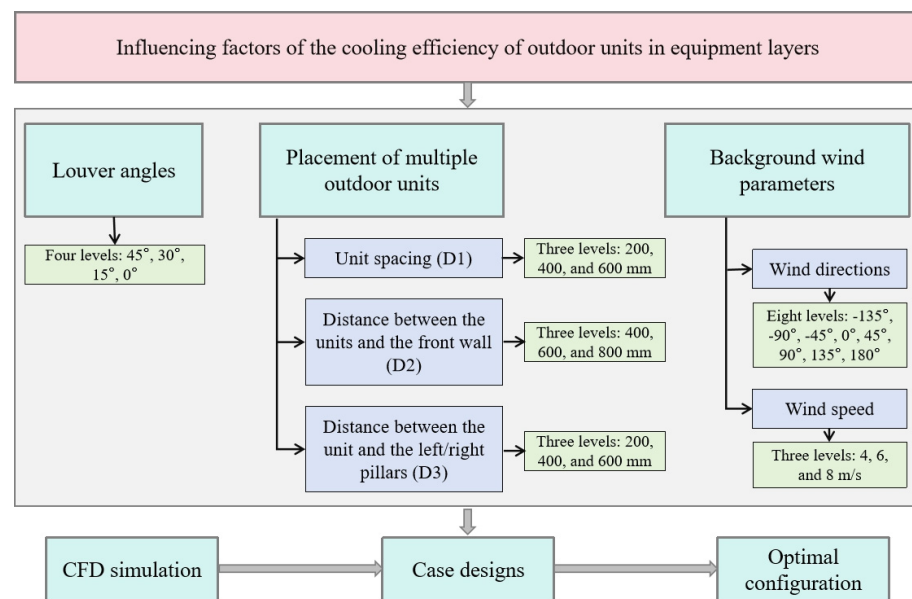
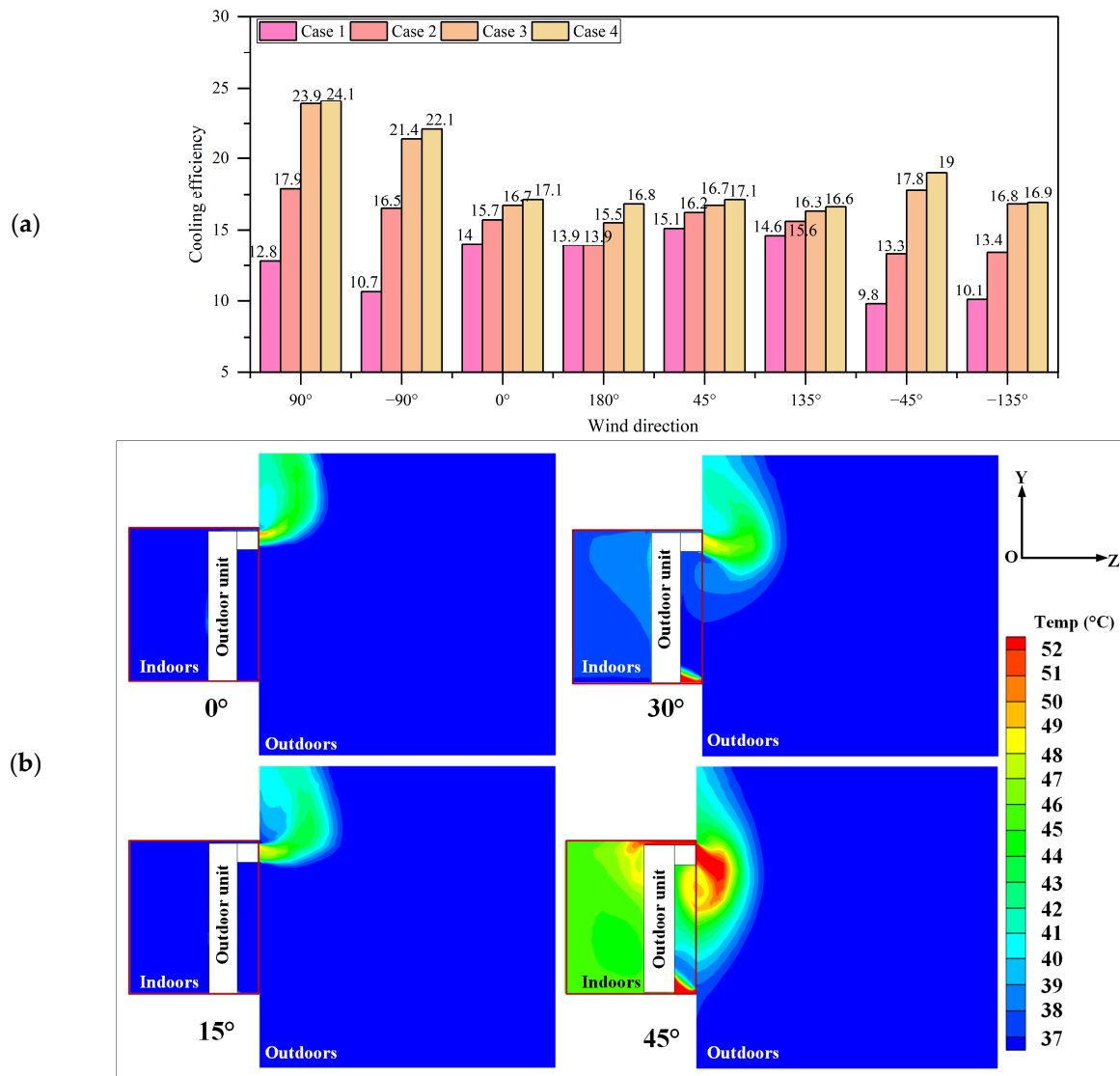


Figure 4. The flowchart of this study.

## 3. Results and Discussion

### 3.1. Louver Angle

Figure 5a shows the changes in the average cooling efficiency of outdoor units when the louver angles ranged from 45° to 0° under eight wind directions. With the louver angles decreased (from Case 1 to Case 4), the average cooling efficiency of outdoor units showed an increasing trend. For example, at a wind direction of 90°, the average cooling efficiency was 12.8, 17.9, 23.9, and 24.1 when the louver angles were 45°, 30°, 15°, and 0°, respectively. The most significant difference in average cooling efficiency was 11.4 when the louver angles ranged from 45° to 0°, and the wind directions were 90° and −90°.



**Figure 5.** Average cooling efficiency and temperature cloud maps of outdoor units under different louver angles ( $0^\circ$ – $45^\circ$ ). (a) average cooling efficiency, (b) temperature cloud maps with  $90^\circ$  wind direction.

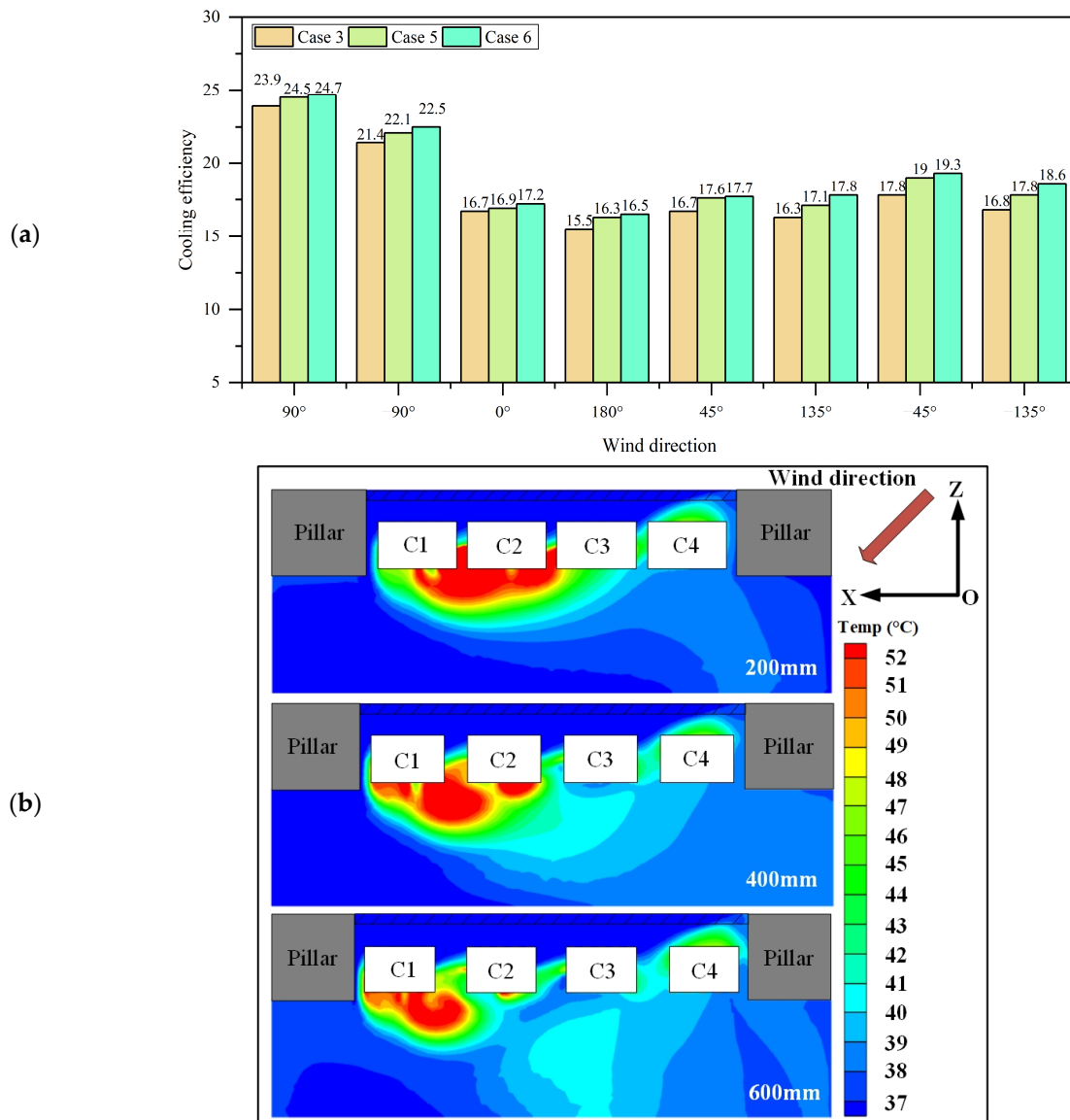
Figure 5b shows the air temperature distribution cloud maps when the wind direction was  $90^\circ$ . The distribution range involved in high temperatures is relatively wide when the louver angles are larger. When the louver angles ranged from  $45^\circ$  to  $0^\circ$  under a  $90^\circ$  wind direction, the air temperature difference was  $14.9^\circ\text{C}$ . Additionally, when the louver angle changed from  $15^\circ$  to  $0^\circ$ , the overall air temperature difference was much smaller compared with others. In practical engineering, louvers are always used in ventilation, air exchange, and rainproofing. Therefore, the louver angle was not recommended to be set as  $0^\circ$  for rainproofing. Then, a  $15^\circ$  louver angle was recommended in the letter cases.

### 3.2. Placement of Outdoor Units

#### 3.2.1. Unit Spacing

Figure 6a shows the changes in the average cooling efficiency of outdoor units when unit spacing ranges from 200 to 600 mm under eight wind directions. The results show that the average cooling efficiency of outdoor units increases with the unit spacing (Case 3, Case 5, and Case 6). For example, at the wind direction of  $90^\circ$ , the air inlet air temperatures were 23.9, 24.5, and 24.7 when the unit spacing was 200, 400, and 600 mm, respectively.

The biggest difference in the average cooling efficiency was 1.5 when the wind direction was 135°.



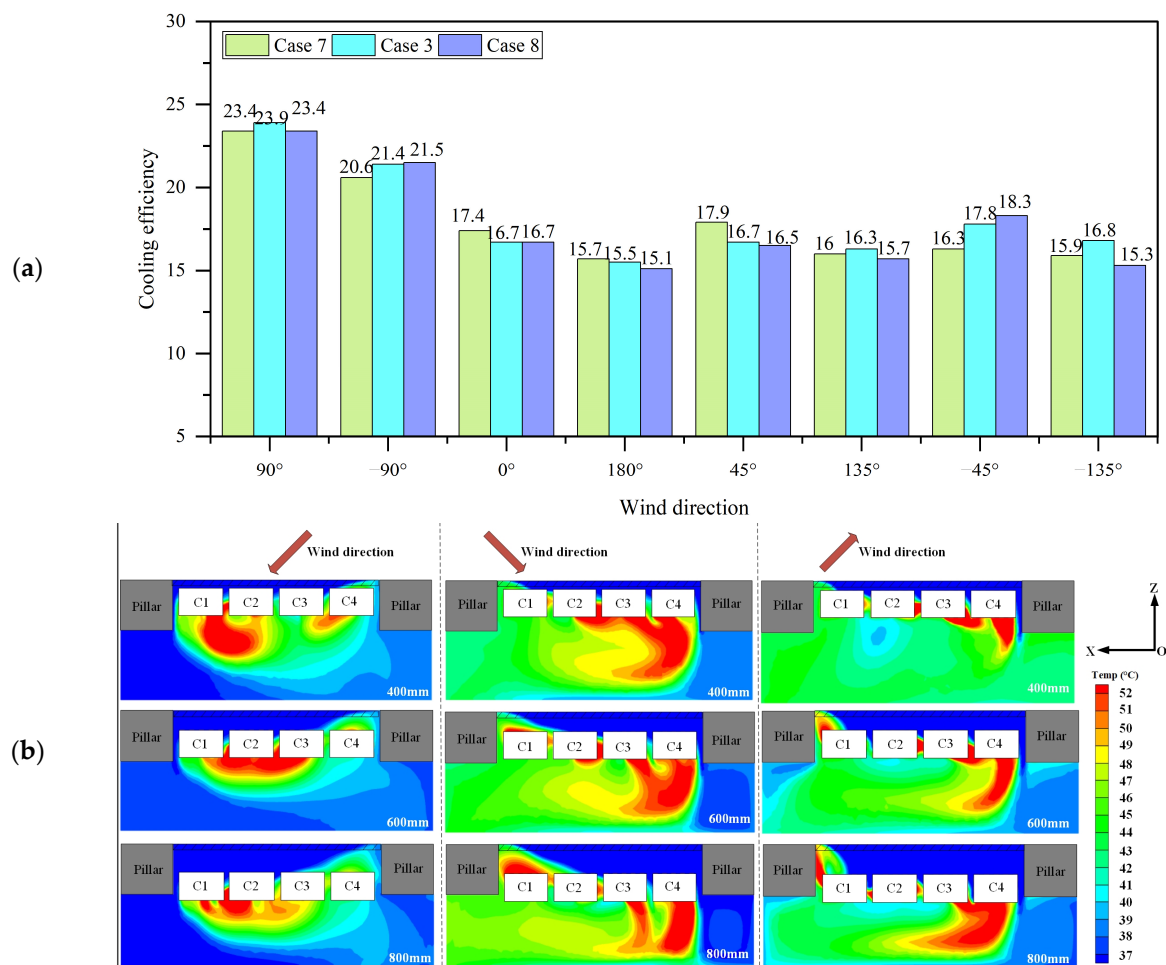
**Figure 6.** Average cooling efficiency and temperature cloud maps under different unit spacings. (a) average cooling efficiency, (b) temperature cloud maps with 135° wind direction and  $Y = 2.65$  m.

Figure 6b shows the air temperature distribution cloud maps with 135° wind direction under different unit spacings. The air temperature difference was 1.7 °C as the unit spacing ranged from 200 to 600 mm. Additionally, the larger the unit spacing, the smaller the distribution of high-temperature areas (see red areas). The high-temperature regions moved to the downwind side with increased unit spacing. For example, the red areas were close to units C1~C3 when the unit spacing was 200 mm, while the areas were close to unit C1 when the unit spacing was 600 mm.

### 3.2.2. Distance Between the Units and the Front Wall

Figure 7a shows the changes in the average cooling efficiency of outdoor units when the distance between the units and the front wall ranges from 400 to 800 mm under eight wind directions. The results show that as the distance between the units and the front wall increases (Case 7, Case 3, and Case 8), the average cooling efficiency of outdoor units displays different changing trends. When wind directions were 90°, 135°, and -135°, the

average cooling efficiency of outdoor units first increased and then decreased. When wind directions were  $-90^\circ$  and  $-45^\circ$ , the average cooling efficiency of outdoor units increased. When wind directions were  $0^\circ$ ,  $180^\circ$  and  $45^\circ$ , the average cooling efficiency of outdoor units decreased. For example, at the wind direction of  $135^\circ$ , the average cooling efficiency of outdoor units was 16, 16.3, and 15.7 when the distance between the units and the front wall was 400, 600, and 800 mm, respectively. At a wind direction of  $-45^\circ$ , the average cooling efficiency of outdoor units was 16.3, 17.8, and 18.3 when the distance between the units and the front wall was 400, 600, and 800 mm, respectively. At a wind direction of  $45^\circ$ , the average cooling efficiency of outdoor units was 17.9, 16.7, and 16.5 when the distance between the units and the front wall was 400, 600, and 800 mm, respectively. Among them, the biggest average cooling efficiency of outdoor units was 2.



**Figure 7.** Average cooling efficiency and temperature cloud maps under different distances between the units and the front wall (400~800 mm). (a) average cooling efficiency, (b) temperature cloud maps with three wind directions ( $135^\circ$ ,  $45^\circ$ , and  $-45^\circ$ ) and  $Y = 2.65$  m.

Figure 7b shows the air temperature distributions with three wind directions ( $135^\circ$ ,  $45^\circ$ , and  $-45^\circ$ ) under different distances between the units and the front wall. The air temperature difference was  $1.7^\circ\text{C}$  when the distance between the units and the front wall ranged from 400 to 800 mm. Similarly, the higher the inlet air temperature, the larger the distribution of high-temperature areas, namely the red regions. Additionally, high-temperature regions occurred on the downwind side.

### 3.2.3. Distance Between the Unit and the Left/Right Pillars

Figure 8a shows the changes in the average cooling efficiency of outdoor units when the distance between the unit and the left/right pillars ranged from 200 to 600 mm under eight wind directions. The results show that as the distance between the units and the left/right pillars increases (Case 3, Case 9, and Case 10), the average cooling efficiency of outdoor units displays different changing trends. When wind directions were  $90^\circ$ ,  $-45^\circ$ , and  $-135^\circ$ , the average cooling efficiency of outdoor units first increased and then decreased. When wind directions were  $0^\circ$ ,  $180^\circ$ ,  $45^\circ$ ,  $135^\circ$ , and  $-90^\circ$ , the average cooling efficiency of outdoor units increased. For example, when the wind direction was  $90^\circ$ , the average cooling efficiency of outdoor units was 23.9, 24.3, and 22.8 when the distance between the unit and the left/right pillars was 200, 400, and 600 mm, respectively. When the wind direction was  $0^\circ$ , the average cooling efficiency of outdoor units was 16.7, 17.2, and 18.2 when the distance between the unit and the left/right pillars was 200, 400, and 600 mm, respectively. Among them, the biggest difference in the average cooling efficiency of outdoor units was 2.5 as the distance between the unit and the left/right pillars ranged from 200 to 600 mm and wind direction was  $-90^\circ$ .

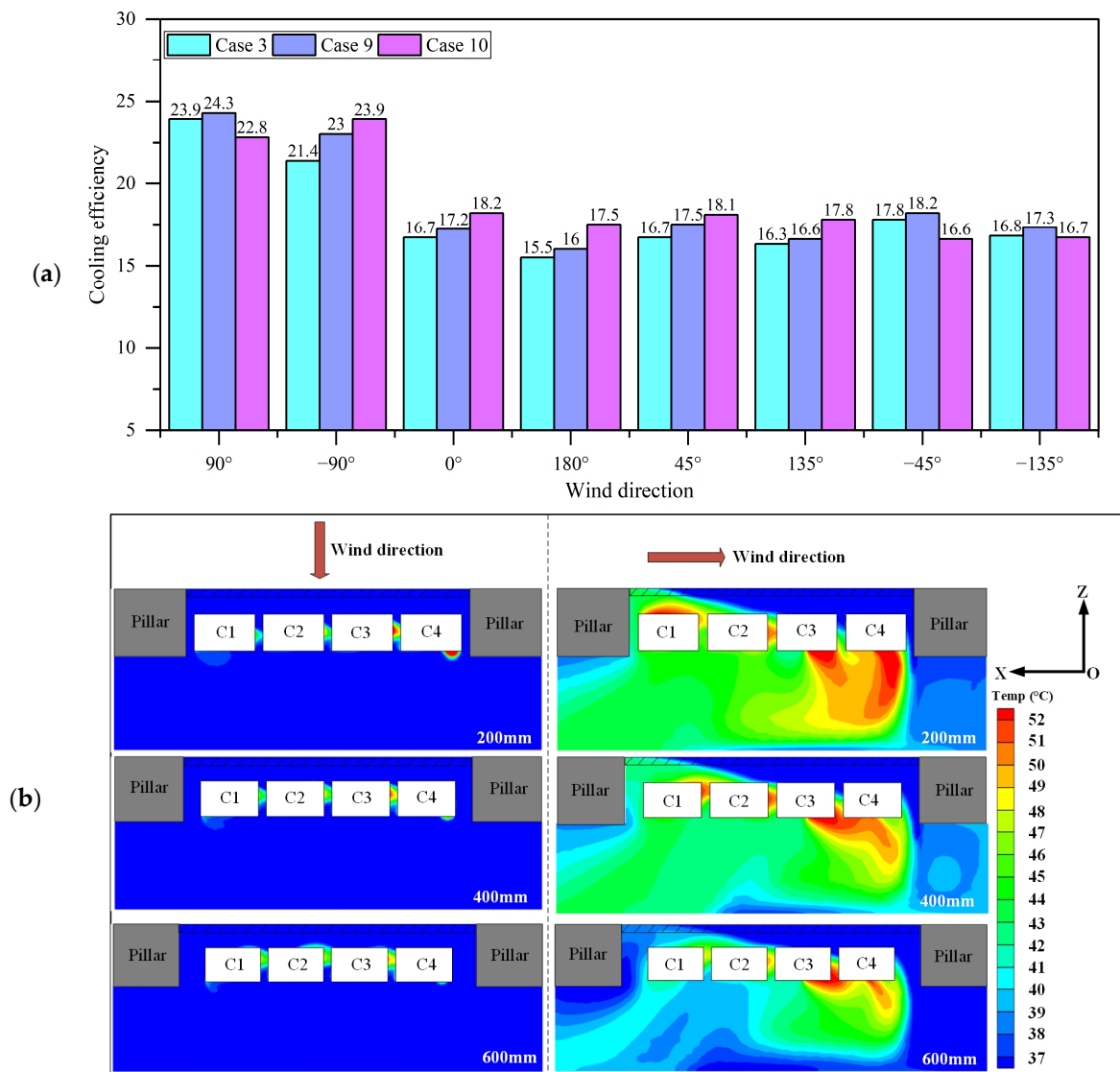


**Figure 8.** Average cooling efficiency and temperature cloud maps under different distances between the units and the left/right pillars (200~400 mm). (a) average cooling efficiency, (b) temperature cloud maps with  $90^\circ$  and  $0^\circ$  of wind directions and  $Y = 2.65$  m.

Figure 8b shows the air temperature distributions with  $90^\circ$  and  $0^\circ$  of wind directions under different distances between the units and the front wall. Similarly, the higher the inlet air temperature, the larger the distribution of high-temperature areas, namely the red regions.

### 3.3. Wind Parameters

Figure 9a shows the changes in the average cooling efficiency of outdoor units when wind speeds ranged from 4 to 8 m/s under eight wind directions. The results show that with wind speed increases (Case 11, Case 3, and Case 12), the average cooling efficiency of outdoor units displayed different changing trends. When wind directions were  $90^\circ$ ,  $180^\circ$ ,  $135^\circ$  and  $-135^\circ$ , the average cooling efficiency of outdoor units first increased and then decreased. When wind directions were  $0^\circ$  and  $-45^\circ$ , the average cooling efficiency of outdoor units increased. When wind directions were  $-90^\circ$  and  $45^\circ$ , the average cooling efficiency of outdoor units first increased and then remained unchanged. For example, when the wind direction was  $90^\circ$ , the average cooling efficiency of outdoor units was 14.9, 23.9, and 22.5 when wind speeds were 4, 6, and 8 m/s, respectively. When the wind direction was  $0^\circ$ , the average cooling efficiency of outdoor units was 16.6, 16.7, and 16.9 when wind speeds were 4, 6, and 8 m/s, respectively. When the wind direction was  $-45^\circ$ , the average cooling efficiency was 17.4, 17.8, and 18 when wind speeds were 4, 6, and 8 m/s, respectively. Among them, the most significant difference in the average cooling efficiency of outdoor units was 9 when the wind direction was  $90^\circ$ .

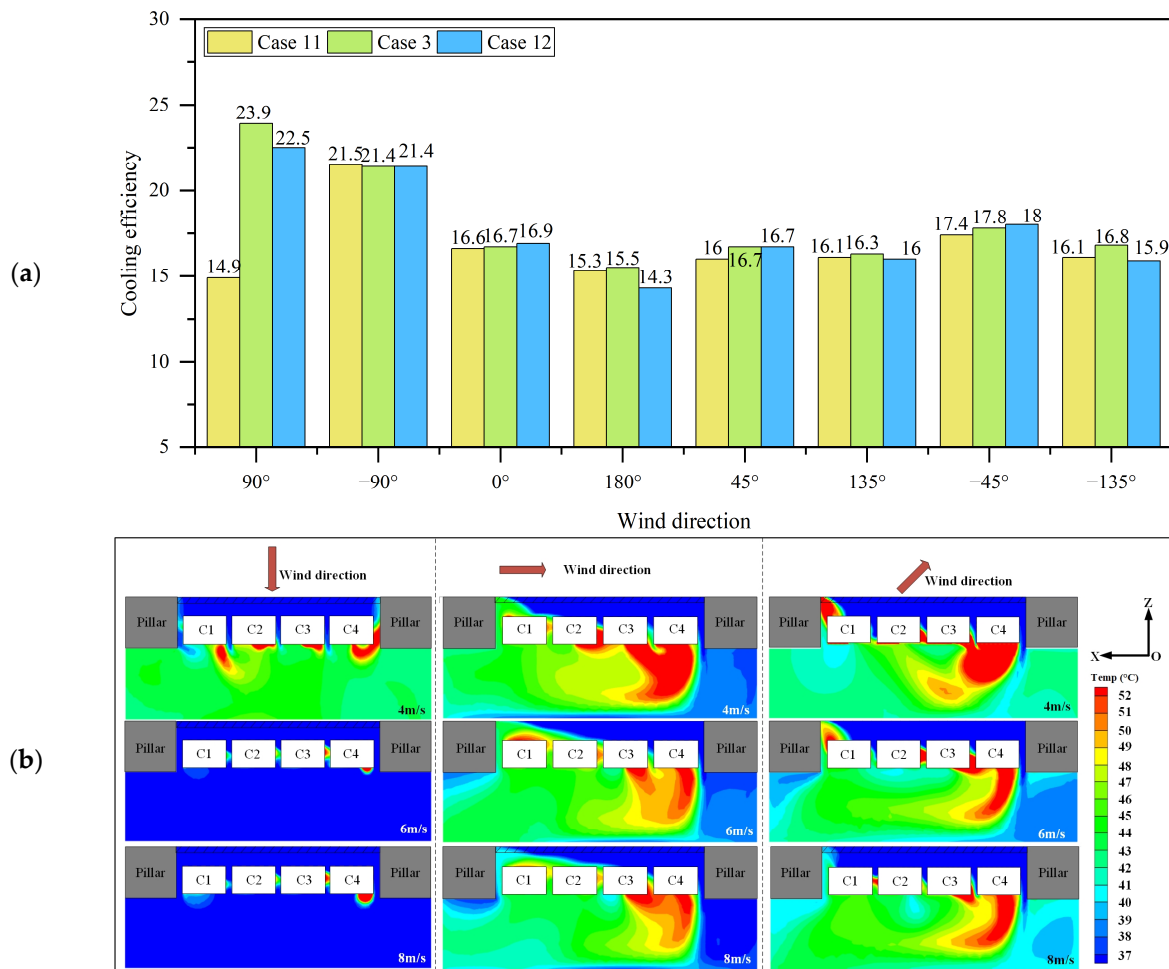


**Figure 9.** Average cooling efficiency and temperature cloud maps under different wind speeds (4~8 m/s). (a) average cooling efficiency, (b) temperature cloud maps with  $90^\circ$ ,  $0^\circ$ , and  $-45^\circ$  wind directions and  $Y = 2.65$  m.

Figure 9b shows the air temperature distributions with  $90^\circ$ ,  $0^\circ$ , and  $-45^\circ$  wind directions under different wind speeds. The biggest air temperature difference was  $7.6^\circ\text{C}$  as wind speeds ranged from 4 to 8 m/s. Similarly, the higher the inlet air temperature, the larger the distribution of high-temperature areas, namely the red regions.

As shown in Figures 4–8, the average cooling efficiency of outdoor units was 21.8, 20.7, 16.7, 15.5, 16.9, 16.3, 17, and 16 as the wind direction was  $90^\circ$ ,  $-90^\circ$ ,  $0^\circ$ ,  $180^\circ$ ,  $45^\circ$ ,  $135^\circ$ ,  $-45^\circ$ ,  $-135^\circ$ , respectively. The corresponding mean overall inlet air temperatures were 40.5, 41.2, 44, 45.3, 43.7, 44.4, 44.3, and  $45.3^\circ\text{C}$ , respectively. The mean overall inlet air temperature at a  $90^\circ$  wind direction was the lowest. The second was a  $-90^\circ$  wind direction, and the biggest one occurred at a  $180^\circ$  wind direction. Among them, the biggest difference in air temperature was  $15.3^\circ\text{C}$  at  $-90^\circ$  in the direction of the wind.

## 4. Discussion

### 4.1. Optimal Configurations

This study adopted a CFD simulation method to explore the effects of multiple factors on the cooling efficiency of VRV systems' outdoor units at the equipment layer in high-rise buildings. These factors include the louver angle, unit spacing, distance between the units and the front wall, distance between the units and the left/right pillars, wind speed, and wind direction. Through CFD simulation, the results showed that these factors have effects on the cooling efficiency of outdoor units to a certain extent. Firstly, it can be seen from Figures 4–8 that the louver angle and wind direction have a relatively significant impact on the cooling efficiency compared with the other factors. For example, the maximum cooling efficiency occurred when the louver angle was  $0^\circ$  and the wind direction was  $90^\circ$  (Figure 5a). The biggest air temperature difference was  $14.9^\circ\text{C}$  as the louver angles ranged from  $45^\circ$  to  $0^\circ$ , and the corresponding cooling efficiency increased by 1.3. Secondly, the factor that had a relatively higher impact on cooling efficiency was wind speed. When wind speeds ranged from 4 to 8 m/s with  $90^\circ$  wind direction, the biggest difference in the average cooling efficiency of outdoor units was 9, and the air temperature difference was  $7.6^\circ\text{C}$  (see Figure 9a). Thirdly, placing multiple outdoor units at the equipment layer has a relatively lower impact on the average cooling efficiency and the overall inlet air temperature. When considering a factor, the maximum cooling efficiency difference could be reduced by 1.5 (see Figures 5a and 6a).

The angle of the louver is linearly correlated with the average cooling efficiency of outdoor units. When the angle of the louver decreases, the average cooling efficiency of outdoor units increases (see Figure 5). Correlation analysis shows a significant positive correlation between the two, with a 0.631 correlation coefficient ( $p < 0.01$ ). Some studies found that the inlet air temperature increases as the inclination angle of the louvers increases [18,19]. Considering the functions of louvers and CFD simulation results, a  $15^\circ$  louver angle can be recommended as the optimal parameter, which ensures a better heat exchange performance and a rain-proof function. Some similar results were found in previous studies. These studies observed that the larger the angle of the louver, the worse the working performance of VRV air conditioning systems. Additionally, the recommended louver angle should not exceed  $20^\circ$ , and the optimal recommended value was  $15^\circ$  [20,33].

As shown in Figures 4–8, when the wind directions were  $90^\circ$  and  $-90^\circ$ , the average cooling efficiency was relatively higher compared with other wind directions. In most cases, the average cooling efficiency in the  $90^\circ$  wind direction was highest compared with that in the  $-90^\circ$  wind direction. Among them, the temperature difference between  $90^\circ$  and  $-90^\circ$  wind directions ranged from  $0.5\text{--}1.7^\circ\text{C}$  in most cases. However, when wind speed was 6 m/s and 8 m/s, the average cooling efficiency of outdoor units in the  $90^\circ$  wind direction was significantly higher than in the  $-90^\circ$  wind direction (see Figure 9). Consequently, considering the dominant wind direction around the selected building, the louvers on the equipment layer can be oriented perpendicular to the wind direction ( $90^\circ$ ) when the wind speed is not less than 6 m/s or the wind direction ( $-90^\circ$ ) when wind speed was less than 6 m/s. According to the calculation formula for wind speed at different building



heights (see Table 5), the equipment layer's height was 177.2 m (39~51 floors) when the wind speed was 6 m/s. In this study, the prevailing wind direction around the selected building is southeast. That is, the louver can be installed in the southwest direction of the building when the equipment layer' is higher than 177.2 m. When the equipment layer is less than 177.2 m, the louver can be installed in the northeast direction of the building. Some studies found similar results. For example, Choi et al. observed that the performance of the condensers could decrease when the floors were higher than 30th or the frontal- and side-wind speeds were greater than 4 m/s and 8 m/s, respectively [39].

Subsequently, as shown in Figure 6, the average cooling efficiency of outdoor units increased with the increase in unit spacing. However, for the distance between the units and the front wall and the distance between the units and the left/right pillars, no consistent changing trends were observed in the average cooling efficiency. In general, 600 mm can be recommended as the optimal distance between the units and the front wall vs. the left/right pillars, according to results from Figures 6 and 7. For example, when determining the louver angle, the equipment layer, and their placement directions, the average cooling efficiency of Case 3 was 0.4 higher than Case 7 and Case 8. The recommended values were consistent with other studies. For example, the distance between the outdoor unit condenser and the wall was greater than 100 mm [33], and the distance between the left side of the outdoor unit and the wall was at least 200 mm [33]. Zhang found that the maximum distance from the pillar is 0.8 m [35]. Based on the above results, when the cooling efficiency was maximum, the optimal parameter configuration was a 15° louver angle. The louvers on the equipment layer could be oriented perpendicular to the wind direction (90°) when the wind speed was not less than 6 m/s, or the wind direction (−90°) when wind speed was less than 6 m/s, the unit spacing was 600 mm, the distance between the units and the front wall was 600 mm, and the distance between the units and the left/right pillars was 400 or 600 mm.

Considering that the influencing degree of louvers and wind parameters were relatively higher, the louver angle was designed as 15°, and the louvers on the equipment layer were oriented perpendicular to the wind direction (90°) in practical scenarios. Based on the CFD simulation results, a multiple linear regression formula was established by taking unit spacing, the distance between the units and the front wall, the distance between the unit and the left/right pillars, and wind speed as the input parameters, and the average cooling efficiency and overall inlet air temperature were taken as dependent variables. Then, the regression formulas of the average cooling efficiency and overall inlet air temperature can be expressed as

$$T_z = 36.671 - 0.001 \times D1 + 0.001 \times D2 + 0.0001 \times D3 \quad (R^2 = 0.735) \quad (7)$$

$$\bar{\varepsilon} = 27.194 + 0.003 \times D1 - 0.001 \times D2 + 0.0001 \times D3 \quad (R^2 = 0.739) \quad (8)$$

According to the regression formulas,  $T_z$  and  $\bar{\varepsilon}$  were 36.731 °C and 28.454, respectively.

#### 4.2. Optimization Schemes

Through the above analysis, the optimal parameter configuration was obtained when outdoor units showed a single-row arrangement at the equipment layer. However, in practical application, considering the increases in cooling/heating demands, the outdoor units in the equipment layer need to be expanded. Due to space limitations and the optimal parameter configuration, six outdoor units can be placed. Considering those possible arrangements for outdoor units in the equipment layer, six layouts were used for further analysis, as shown in Figure 10a. Among them, Layout 1 is that six outdoor units were in a single row. Layout 2 is that six outdoor units are arranged in a double row and a parallel arrangement. Layout 3~6 is that six outdoor units are arranged in a double row and staggered patterns. The heat exchange surfaces of Layout 3~4 were different from that of Layout 5~6. Among them, Layouts 3 and 4 showed staggered arrangements in the same direction as the heat exchange surfaces of all units. Layouts 5 and 6 showed a staggered

arrangement of units with the different directions of the heat exchange surfaces of all units. The distances between units in different rows were 600, 800, and 1000 mm, respectively.

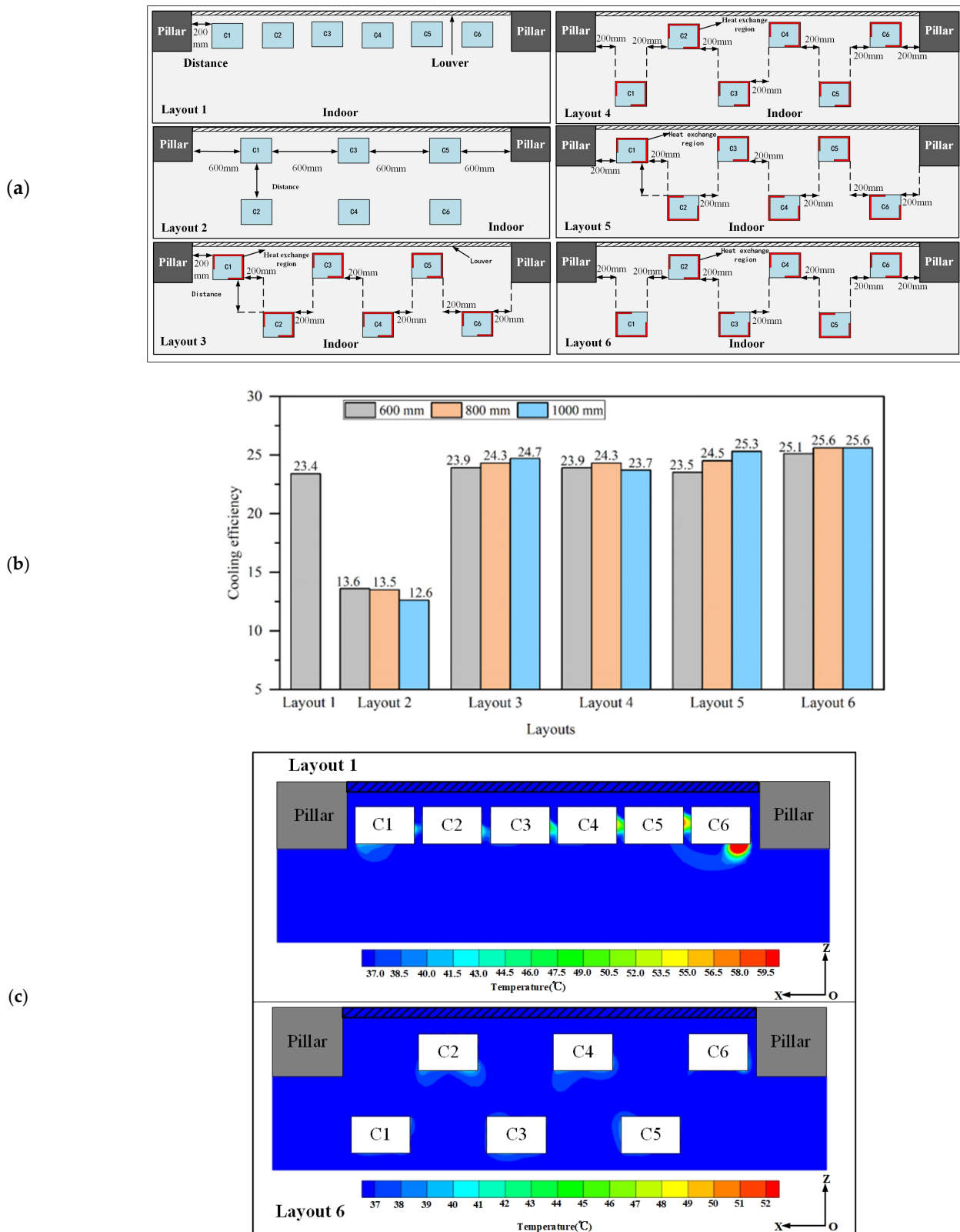


Figure 10. Outdoor units under different layouts. (a) Arrangement of outdoor units. (b) Average cooling efficiency. (c) air temperature distribution cloud maps.

Figure 10b shows the average cooling efficiency of outdoor units with the optimal parameter configurations under different layouts. The average cooling efficiency of outdoor units was lowest when outdoor units were in a parallel arrangement (Layout 2) compared with other layouts. Compared with the single row, the average cooling efficiency of outdoor units showed higher values in double arrangements (see Layouts 3, 4, 5, and 6). Under Layouts 3, 5, and 6, the average cooling efficiency of outdoor units showed an increasing trend with the distances between units in different rows increased. For Layout 4, the average cooling efficiency of outdoor units occurred when the distance was 800 mm. Besides that, when the average cooling efficiency of outdoor units was maximum, the optimal layout was Layout 6. Figure 10c shows the air temperature distribution cloud maps of Layout 1 and Layout 6. Ge et al. found that compared with units showing the same side of exhaust air, the units with the opposite side of exhaust air show a better performance [42].

## 5. Conclusions and Future Works

### 5.1. Main Conclusions

This study investigates an optimization parameter configuration that produces a higher heat exchange efficiency of outdoor units placed in the equipment layer on the high floors of buildings. The relevant parameters include three aspects: wind parameters, the placement of outdoor units, and the louver. Among them, wind parameters include outdoor wind speed and wind direction. The placements of outdoor units are unit spacing, the distance between the units and the front, and the distance between the unit and the left/right pillar. A total of 96 cases were designed based on these factors, including four louver angles ( $45^\circ$ ,  $30^\circ$ ,  $15^\circ$ ,  $0^\circ$ ), three unit spacings (200, 400, and 600 mm), three distances between the unit and the left/right columns (200, 400, and 600 mm), three distances between the units and the front wall (400, 600, and 800 mm), three wind speeds (4, 6, and 8 m/s), and eight wind directions ( $-135^\circ$ ,  $-90^\circ$ ,  $-45^\circ$ ,  $0^\circ$ ,  $45^\circ$ ,  $90^\circ$ ,  $135^\circ$ ,  $180^\circ$ ). The CFD simulation method was used to obtain the inlet air temperature distributions of multiple outdoor units in the equipment layers, and then the average cooling efficiency of outdoor units was calculated. The main conclusions are as follows:

Firstly, these factors have effects on the average cooling efficiency of outdoor units in a single row to a certain extent. Among them, the angle of the louver and wind direction have a relatively significant impact on the average cooling efficiency and overall inlet air temperature compared with other factors. The average cooling efficiency increased by 11.4 as the angle of the louver ranged from  $45^\circ$  to  $0^\circ$ . When wind speeds ranged from 4 to 8 m/s, the average cooling efficiency increased by 1.5 when the wind direction was  $135^\circ$ . However, placing multiple outdoor units at the equipment layer has a relatively lower impact on the average cooling efficiency and overall inlet air temperature.

Secondly, when the cooling efficiency was maximum, the optimal parameter configuration and the order of configuration were: (1) a louver angle was set as  $15^\circ$ , (2) the louvers on the equipment layer could be oriented perpendicular to the wind direction ( $90^\circ$ ) when wind speed was not less than 6 m/s, or the wind direction ( $-90^\circ$ ) when wind speed was less than 6 m/s, (3) the unit spacing was 600 mm, (4) the distance between the units and the front wall was 600 mm, and (5) the distance between the units and the left/right pillars was 400 or 600 mm.

Thirdly, when the number of outdoor units was expanded in the limited equipment layer, the recommended optimization schemes for the layout of outdoor units were that the outdoor units showed a staggered arrangement and the direction of the heat exchange surfaces of all units were different (Layout 6).

### 5.2. Limitations and Future Works

This study provides a parametric and systematic optimization design method for obtaining a better heat exchange performance of multiple outdoor units placed in an equipment layer of high-rise buildings. The results of this study can effectively guide the designs of practical engineering projects to save building energy consumption and reduce

economic costs. Importantly, the proposed optimal configurations can be generalized to other climates. However, for different air conditioning systems, the optimal configurations could be different due to the different working power levels.

During CFD simulations, the wall was assumed to be insulated without considering the effects of outdoor solar radiation. Actually, outdoor solar radiation increases indoor heat gain to a certain degree [51,52]. The increased heat gain exacerbates the rise in the indoor air temperature at the equipment layer. There may be a coupling effect between the increased air temperature and the outdoor unit's heat dissipation, which then influences the temperature distribution, thus leading to the rise in building energy consumption, economic, and carbon saving [53]. Thus, it is necessary to explore the impact of outdoor solar radiation in the future. Additionally, experiments will be conducted to validate the effectiveness of the CFD simulation results of this study, and the placements of outdoor units will be further optimized when the space is limited. This study used only typical wind speeds to explore the impacts on system performance. More experiments would be conducted to examine the effects of seasonal wind variations on long-term system performance and to verify the validation of these results.

Besides that, in this study, the optimization of cooling efficiency focuses on airflow, louver angles, and spatial arrangements. In the future, other factors, including the perovskite smart windows [54], noise, maintenance, and installation costs, will be considered.

**Author Contributions:** Conceptualization, L.L., H.H. and X.T.; methodology: H.H.; software, H.H.; formal analysis, X.T.; data curation: H.H.; writing—original draft preparation, L.L.; writing—review and editing, X.T.; visualization, X.T.; supervision, L.L. and X.T.; project administration, L.L.; funding acquisition, L.L. All authors have read and agreed to the published version of the manuscript.

**Funding:** This research was funded by National Natural Science Foundation of China (Grant No. 52208099).

**Data Availability Statement:** The data presented in this study are available on request from the corresponding author.

**Conflicts of Interest:** The authors declare no conflicts of interest.

## Nomenclature

CFD	Computational Fluid Dynamics	$T_0$	cooled temperature
CO <sub>2</sub>	Carbon dioxide	$T_k$	temperature of the heat source
Gt	Grand Tourer	$T_Z(m + 1)/T_Z(m)$	Mean inlet temperature of (m + 1)th/mth iteration
TWh	Tera Watt Hour	$Q_i$	cooling capacity ratio
VRV	Variable Refrigerant Volume	$Q_z$	the total cooling capacity
hc	reference height, which is 10 m	$V_c$	wind speed of reference height, which is 1.9 m/s.
h	a height.	$V$	wind speed at a height.
n	Roughness index, which is set as 0.4.	$\varepsilon$	refrigeration machine
T-S diagram	Temperature- Entropy diagram	$\bar{\varepsilon}$	average cooling efficiency of refrigeration machine

## References

1. Tian, X.; Zhang, H.; Liu, L.; Huang, J.; Liu, L.; Liu, J. Establishment of LCZ-based urban building energy consumption dataset in hot and humid subtropical regions through a bottom-up method. *Appl. Energy* **2024**, *368*, 123491. [CrossRef]
2. Kang, C.; Zhou, T.; Chen, Q.; Xu, Q.; Xia, Q.; Ji, Z. Carbon emission flow in networks. *Sci. Rep.* **2012**, *2*, 479. [CrossRef] [PubMed]
3. Zheng, S.; Huang, G.; Zhou, X.; Zhu, X. Climate-change impacts on electricity demands at a metropolitan scale: A case study of Guangzhou, China. *Appl. Energy* **2020**, *261*, 114295. [CrossRef]
4. World Bank Group. CO<sub>2</sub> Emissions. 2023. Available online: <https://data.worldbank.org/topic/climate-change> (accessed on 30 September 2024).
5. UN Environment Programme. *2022 Global Status Report for Buildings and Construction: Towards a Zero-Emission, Efficient and Resilient Buildings and Construction Sector*; Springer: Berlin/Heidelberg, Germany, 2023. [CrossRef]

6. Xiaoqing, Z.; Fang, L.; Weiqing, C.; Shurong, Y.; Yunfei, D. Investigation and study on energy consumption of public buildings in Guangzhou. *Build. Sci.* **2007**, *23*, 76–80.
7. Zhen, L. *Chongqing High-Level Office Buildings Air Conditioning Load Characteristic and Energy Consumption Analysis Research*; College of Faculty of Urban Construction and Environment Engineering Chongqing University: Chongqing, China, 2007.
8. Zhao, D.; Zhong, M.; Zhang, X.; Su, X. Energy consumption predicting model of VRV (Variable refrigerant volume) system in office buildings based on data mining. *Energy* **2016**, *102*, 660–668. [[CrossRef](#)]
9. Hu, Y.; Zhang, Y.; Liu, X.; Li, H. Development and demonstration of a method to detect refrigerant charge level for variable refrigerant volume systems. *Appl. Therm. Eng.* **2023**, *235*, 121354. [[CrossRef](#)]
10. Helbling, M.; Meierrieks, D. Global warming and urbanization. *J. Popul. Econ.* **2023**, *36*, 1187–1223. [[CrossRef](#)]
11. Liu, L.; Pan, X.; Jin, L.; Liu, L.; Liu, J. Association analysis on spatiotemporal characteristics of block-scale urban thermal environments based on a field mobile survey in Guangzhou, China. *Urban Clim.* **2022**, *42*, 101131. [[CrossRef](#)]
12. Kabeel, A.E.; Abdelgaied, M.; Sathyamurthy, R.; Arunkumar, T. Performance improvement of a hybrid air conditioning system using the indirect evaporative cooler with internal baffles as a pre-cooling unit. *Alexandria Eng. J.* **2017**, *56*, 395–403. [[CrossRef](#)]
13. Yau, Y.H.; Pean, H.L. The performance study of a split type air conditioning system in the tropics, as affected by weather. *Energy Build.* **2014**, *72*, 1–7. [[CrossRef](#)]
14. Chow, T.T.; Lin, Z.; Yang, X.Y. Placement of condensing units of split-type air-conditioners at low-rise residences. *Appl. Therm. Eng.* **2002**, *22*, 1431–1444. [[CrossRef](#)]
15. Chow, T.T.; Lin, Z.; Liu, J.P. Effect of condensing unit layout at building re-entrant on split-type air-conditioner performance. *Energy Build.* **2002**, *34*, 237–244. [[CrossRef](#)]
16. Nada, S.A.; Said, M.A. Solutions of thermal performance problems of installing AC outdoor units in buildings light wells using mechanical ventilations. *Appl. Therm. Eng.* **2018**, *131*, 295–310. [[CrossRef](#)]
17. Xue, H.; Chou, S.K.; Zhong, X.Q. Thermal environment in a confined space of high-rise building with split air conditioning system. *Build. Environ.* **2004**, *39*, 817–823. [[CrossRef](#)]
18. Cheng, Z.; Huang, Z.; Ma, Y. Influence of pitch angle of the louver leaves on outdoor unit's operating conditions of air conditioners. *HV&AC* **2009**, *39*, 133–135.
19. Yang, Y. The effect of shutter's parameter on performance of VRF air conditioning system. *Build. Energy Environ.* **2017**, *36*, 34–37.
20. Liu, W.; Xie, X.; Li, N. Experimental research on influence of louver angle on performance of air conditioner's outdoor unit. *Refrig. Air-Cond.* **2017**, *17*, 37–39.
21. Yang, Y.; Cheng, Y.; Liu, B.; He, K.; Hai, X. CFD analysis and optimization of thermal environment for outdoor unit of air conditioner at groove in a commercial building. *HV&AC* **2016**, *46*, 33–35.
22. Chow, T.T.; Lin, Z.; Wang, Q.W. Flow analysis of condenser cooling air delivery via building light well. *Appl. Therm. Eng.* **2001**, *21*, 831–843. [[CrossRef](#)]
23. Nada, S.A.; Said, M.A. Performance and energy consumptions of split type air conditioning units for different arrangements of outdoor units in confined building shafts. *Appl. Therm. Eng.* **2017**, *123*, 874–890. [[CrossRef](#)]
24. Yiqi, L. The Influence of the Operating Environment and Thermal Environment on the Performance of the Outdoor Air-Conditioner. Master's thesis, Harbin University of Commerce, Harbin, China, 2018.
25. Zhou, D.; Shao, X.; Zhang, X.; Li, X.; Shi, W.; Wang, B. Numerical simulation of thermal environment for outdoor units at building re-entrant. *J. Guangzhou Univ.* **2010**, *9*, 17–22.
26. Zhao, A.; Li, Q.; Meng, Q.; Meng, Q. Experimental Study on the Performance of Air-Cooled Condensing Unit in Groove. In Proceedings of the 2nd International Conference on Sustainable Energy and Environmental Engineering (SEEE 2016), Xiamen, China, 18–19 December 2016. [[CrossRef](#)]
27. Tao, Y.; Ying, Z.; Ying, S.; Peng, T. Simulation and optimization of thermal environment for outdoor units of air conditioner in Groove of a high-rise building. *J. Build. Energy Effic.* **2022**, *50*, 72–77.
28. Huang, S.; Cao, Y.; Li, X.; Pei, Z.; Ni, X.; Wang, S.; Zhou, J.; Wang, Q. CFD simulation and optimization of multi-split air conditioning outdoor unit scheme for a super high-rise building. *HV&AC* **2017**, *47*, 77–82.
29. Avara, A.; Daneshgar, E. Optimum placement of condensing units of split-type air-conditioners by numerical simulation. *Energy Build.* **2008**, *40*, 1268–1272. [[CrossRef](#)]
30. Xue, H.; Xu, B.; Wu, J.; Wei, Y. Prediction of temperature rise near condensing units in the confined space of a high-rise building. *Build. Environ.* **2007**, *42*, 2480–2487. [[CrossRef](#)]
31. Duan, R.; Wang, X.; Song, Y.; Liu, J. Influence of Air-conditioning Outdoor Unit Arrangement Strategy on Energy Consumption. *Procedia Eng.* **2016**, *146*, 350–358. [[CrossRef](#)]
32. Harithkhan, V.M.; Nissanka, I.D.; Manthilake, M.M.I.D. System performance of split type A/C units in high-rise residential buildings with different condenser arrangements. In Proceedings of the MERCon 2022—Moratuwa Engineering Research Conference, Moratuwa, Sri Lanka, 27–29 July 2022; pp. 1–6. [[CrossRef](#)]
33. Jiang, Y. Research on the thermal environment around outdoor unit of split air conditioner. Master's thesis, Tianjin University of Commerce, Tianjin, China, 2013.
34. Bruelisauer, M.; Meggers, F.; Saber, E.; Li, C.; Leibundgut, H. Stuck in a stack—Temperature measurements of the microclimate around split type condensing units in a high rise building in Singapore. *Energy Build.* **2014**, *71*, 28–37. [[CrossRef](#)]

35. Zhang, J. Simulation and Analysis to the Thermal Environment Around the Outdoor Units of VRV Air-Conditioner System. Master's thesis, Dalian University of Technology, Dalian, China, 2009.
36. Jing, Z.; Kun, Z.; Angui, L.; Xiaohong, N. Analysis on optimizing array of air-conditioning condensers. *J. Refrig.* **2008**, *29*, 12–17.
37. Wei, X.; Jiang, P. Simulation and analysis of thermal environment of VRF air-conditioning outdoor units with horizontal array arrangement. *J. Zhejiang Sci.-Technol. Univ.* **2021**, *45*, 149–156.
38. Chow, T.; Lin, Z.; Wang, Q. Effect of building re-entrant shape on performance of air-cooled condensing units. *Energy Build.* **2000**, *32*, 143–152. [[CrossRef](#)]
39. Choi, S.H.; Lee, K.S.; Kim, B.S. Effects of stacked condensers in a high-rise apartment building. *Energy* **2005**, *30*, 968–981. [[CrossRef](#)]
40. Li, H.; Liu, W. Study of position of outdoor units formulti-splits air-conditioning system. *Refrig. Air-Cond.* **2019**, *11*, 82–87.
41. Zi, X.; Wu, S. Optimization design on air-conditioning scheme for on high-rise building. *Refrig. Air-Cond.* **2017**, *17*, 59–64.
42. Fei, G.; Bo, L.; Ming, X. Numerical research on effects of outside unit placement on unit performance for variable refrigerant volume air conditioning systems in multi-storied buildings. *HV&AC* **2007**, *5*, 97–100.
43. Umar, T. Making future floating cities sustainable: A way forward. *Proc. Inst. Civ. Eng. Urban Des. Plan.* **2020**, *173*, 214–237. [[CrossRef](#)]
44. Tippu, J.; Saravanasankar, S.; Sankaranarayanan, B.; Ali, S.M.; Qarnain, S.S.; Karuppiah, K. Towards Sustainability: Analysis of Energy Efficiency Factors in Buildings of Smart Cities Using an Integrated Framework. *J. Inst. Eng. Ser. A* **2023**, *104*, 223–235. [[CrossRef](#)]
45. Chen, R.; Xu, W.; Deng, S.; Zhao, R.; Choi, S.Q.; Zhao, L. Towards the Carnot efficiency with a novel electrochemical heat engine based on the Carnot cycle: Thermodynamic considerations. *Energy* **2023**, *284*, 128577. [[CrossRef](#)]
46. R, T.; Hiremath, N.; Narayanaswamy, K.S. Numerical Studies of Air Flow Analysis in Compressed Air Filters. *J. Mines Met. Fuels* **2022**, *70*, 342. [[CrossRef](#)]
47. Zore, K.; Caridi, D.; Lockley, I. *Fast and Accurate Prediction of Vehicle Aerodynamics Using ANSYS Mosaic Mesh*; SAE Technical Paper; Commercial Vehicle Engineering Congress; October; SAE International: Warrendale, PA, USA, 2019. [[CrossRef](#)]
48. Canonsburg, T.D. ANSYS FLUENT Meshing Text Command List. *Knowl. Creat. Diffus. Util.* **2012**, 15317.
49. Boujelbene, M.; El-Zahar, E.R.; Seddek, L.F.; Ullah, Z.; Makinde, O.D. Viscous dissipation and variable viscosity impacts on oscillatory heat and mass transfer of gravity-driven reactive flow along heated plate. *Phys. Fluids* **2023**, *35*, 073604. [[CrossRef](#)]
50. Guo, T. Study on Layout of VRF Air-Conditioning Outdoor Units Based on CFD Simulation. Master's thesis, Xihua University, Chengdu, China, 2021.
51. Alawadhi, E.M. Effect of an incompletely closed window shutter on indoor illuminance level and heat gain. *Energy Build.* **2016**, *110*, 112–119. [[CrossRef](#)]
52. Bueno, B.; Pigeon, G.; Norford, L.K.; Zibouche, K.; Marchadier, C. Development and evaluation of a building energy model integrated in the TEB scheme. *Geosci. Model Dev.* **2012**, *5*, 433–448. [[CrossRef](#)]
53. Zheng, Z.; Xiao, J.; Yang, Y.; Xu, F.; Zhou, J.; Liu, H. Optimization of exterior wall insulation in office buildings based on wall orientation: Economic, energy and carbon saving potential in China. *Energy* **2024**, *290*, 130300. [[CrossRef](#)]
54. Liu, S.; Du, Y.; Zhang, R.; He, H.; Pan, A.; Ho, T.C.; Zhu, Y.; Li, Y.; Yip, H.L.; Jen, A.K.Y.; et al. Perovskite Smart Windows: The Light Manipulator in Energy-Efficient Buildings. *Adv. Mater.* **2024**, *36*, 2306423. [[CrossRef](#)]

**Disclaimer/Publisher's Note:** The statements, opinions and data contained in all publications are solely those of the individual author(s) and contributor(s) and not of MDPI and/or the editor(s). MDPI and/or the editor(s) disclaim responsibility for any injury to people or property resulting from any ideas, methods, instructions or products referred to in the content.